Homogeneous nucleation in polypropylene and its blends by small-angle light scattering

Z. Bartczak and A. Galeski
Centre of Molecular and Macromolecular Studies, Polish Academy of Sciences, Boczna 5, 90-362 Lodz, Poland
(Received 11 October 1988; revised 7 November 1989; accepted 4 January 1990)

The homogeneous primary nucleation of spherulitic crystallization in isotactic polypropylene (iPP) and its blends with atactic polypropylene (aPP) was studied. Bulk samples of iPP and iPP/aPP blends were crystallized isothermally under high undercoolings ($\sim 100°C$) using a specially designed crystallization cell. In crystallized samples the fifth-order average spherulite radius was determined on the basis of small-angle light scattering measurements. The parameters for homogeneous primary nucleation were obtained from the fitting of curves calculated on the basis of theoretical predictions for regime III to the experimental data. For that purpose the theoretical background for homogeneous nucleation in polymer blends and for small-angle light scattering by an assembly of impinged spherulites was developed. The results obtained for homogeneous nucleation in plain iPP are in very good agreement with theoretical predictions. For iPP/aPP blends it was found that the main reason for depression of nucleation in blends is the additional energy barrier connected with the separation of components of a homogeneous blend during crystallization of one of the components (iPP).

(Keywords: crystallization; homogeneous nucleation; small-angle light scattering; blends, polypropylene)

INTRODUCTION

Polymer blends with crystallizable components are systems of continuously increasing industrial interest. In most cases the crystallizable component of the blend forms the spherulitic structure during its crystallization from the molten state[1]. The mechanical properties of blends depend strongly on the spherulitic structure. The number and the type of primary nuclei of spherulites in the blends, controlling spherulite sizes and size distribution, appears to be of special importance.

In our previous studies[2,3] we have examined the heterogeneous and self-seeding modes of primary nucleation in blends of polymers based on isotactic polypropylene (iPP). The aim of the study reported here was to investigate the homogeneous primary nucleation of iPP spherulites both in plain polymer and in iPP-based blends.

Homogeneous primary nucleation of some pure polymers (including isotactic polypropylene) crystallized from the melt has been investigated by several authors[4–9]. The method used in those investigations was the so-called 'droplet technique' in which the crystallization of a polymer proceeds at very high undercoolings in a sample of polymer prepared in the form of very small, isolated droplets ($\sim 1\ \mu m$ in diameter) dispersed in an inert liquid medium or deposited on a glass surface. The application of such a technique enables direct determination of the number of homogeneous nuclei as well as the kinetics of homogeneous nucleation of a polymer. The results obtained using this technique confirmed generally some previous theoretical predictions for homogeneous nucleation in polymers. However, there was a discrepancy between theoretically predicted and experimentally determined values of the nucleation constant I_0, the pre-exponential factor in the Turnbull–Fisher equation. The experimental values were several orders of magnitude higher than the theoretical ones.

The study of the homogeneous primary nucleation process in polymer blends has not yet been reported. There is an experimental complication in using the droplet technique to study the nucleation process in multicomponent systems—no method of dispersion can assure the uniformity of composition and molecular-weight distribution of components in all droplets. The conditions for nucleation in each droplet would be different and different from those in bulk samples. For this reason, one is rather forced to study the nucleation behaviour in bulk samples. The method developed by us comprises the isothermal crystallization of samples having the form of thin films ($\sim 40\ \mu m$ thick) in a crystallization cell specially designed to achieve very high undercooling. At such undercooling the average spherulite size is much smaller than the sample thickness, so the sample can be considered as a bulk, three-dimensional sample. The spherulite sizes in the sample can be studied by small-angle light scattering (SALS). The nucleation parameters were determined on the basis of SALS measurements performed upon completion of crystallization of the samples. Mathematical expressions for intensity of light scattered by a system of size-distributed and truncated spherulites were developed and used for this purpose.

As an object of investigation the blend of two polypropylene isomers was selected: isotactic (iPP) and atactic (aPP). In this blend iPP constitutes the crystallizing component whereas aPP is unable to crystallize. The advantage of using such a blend is in the rather simple interpretation of experimental data because of the identical chemical composition of both components,

0032-3861/90/112027-12

nearly the same glass transition temperature for both components, and surface energies of iPP crystals independent of the blend composition. For all compositions the mixture of iPP with aPP constitutes a homogeneous system in the molten state, with no phase separation. Samples of plain iPP were additionally studied for comparison.

THEORETICAL BACKGROUND

Homogeneous primary nucleation and spherulite growth rate in blends of compatible polymers

The rate of homogeneous nucleation in a homopolymer melt is usually described by the well known Turnbull–Fisher equation[10,11]:

$$I = I_0 \exp\left(-\frac{\Delta F^*}{kT}\right)\exp\left(-\frac{\Delta G^*}{kT}\right) \quad (1)$$

where I_0 is the nucleation constant, approximated by nkT/h, where n is the number of crystallizing segments per volume unit and k and h are the Boltzman and Planck constants; ΔF^* is the free enthalpy of activation of the transport of crystallizing segments across the melt–crystal interface; and ΔG^* is the free enthalpy of formation of a critical-sized nucleus.

The term ΔF^* is usually approximated by the WLF equation for viscous flow[11]:

$$\frac{\Delta F^*}{kT} = \frac{U^*}{R(T-T_\infty)} \quad (2)$$

where U^* is a constant characterizing the activation energy of viscous flow ($U^* = 4120\,\text{cal mol}^{-1}$) and T_∞ is the hypothetical temperature at which all motion connected with the flow ceases ($T_\infty = T_g - 51.6\,\text{K}$, where T_g is the glass transition temperature).

Assuming a rectangular shape of the nucleus, equation (1) can be expressed in the form:

$$I = I_0 \exp\left(-\frac{U^*}{R(T-T_\infty)}\right)\exp\left(-\frac{32\sigma^2\sigma_e}{(\Delta g_f)^2 kT}\right)$$
$$= I_0 \exp\left(-\frac{U^*}{R(T-T_\infty)}\right)\exp\left(-\frac{32\sigma^2\sigma_e (T_m^\circ)^2}{(\Delta h_f f \Delta T)^2 kT}\right) \quad (3)$$

in which σ and σ_e are the lateral and fold-surface free energies of the lamellae; $\Delta g_f = (\Delta h_f\, \Delta T/T_m^\circ) f$ is the free enthalpy of fusion; Δh_f is the enthalpy of fusion; T_m° is equilibrium melting temperature; $\Delta T = T_m^\circ - T$; and $f = 2T/(T_m^\circ + T)$[10].

Similarly, the equation describing the spherulite growth rate in a plain polymer (controlled by a secondary nucleation process) is:

$$G = G_0 \exp\left(-\frac{U^*}{R(T-T_\infty)}\right)\exp\left(-\frac{4b_0\sigma\sigma_e}{\Delta g_f kT}\right)$$
$$= G_0 \exp\left(-\frac{U^*}{R(T-T_\infty)}\right)\exp\left(-\frac{4b_0\sigma\sigma_e T_m^\circ}{\Delta h_f f \Delta T kT}\right) \quad (4)$$

where G_0 is a constant and b_0 is the distance between two adjacent fold planes. Equation (4) is written here in the form appropriate for regime III crystallization. Isotactic polypropylene crystallizes according to this regime at temperatures lower than 137°C[12].

The homogeneous primary nuclei in the melt of the homogeneous blend have the same nature as in the melt of the homopolymer, hence the equation describing the rate of nucleation in the blend should be similar in form to equation (3). On the other hand, the concentration of macromolecules from which a single nucleus is formed in the blend is lower than that in plain crystallizing polymer. Also different are the conditions of transport of crystallizing segments across the melt–crystal interface, which influences the transport energy barrier. The most important difference between crystallization in plain polymer and homogeneous blend is that crystallization in the blend causes the separation of blend components: the crystalline phase may consist only of macromolecules of one blend component. The additional work performed by the system is connected with that component separation. Taking the above into consideration, we propose the following form of the equation for the rate of homogeneous nucleation in blends:

$$I = I_{0b} \exp\left(-\frac{U^*}{R(T-T_{\infty b})}\right)\exp\left(-\frac{32\sigma^2\sigma_e}{(\Delta g')^2 kT}\right) \quad (5)$$

in which $I_{0b} = I_0 c'$, where I_0 is the nucleation constant representative of crystallizable polymer and c' is a factor dependent on concentration of crystallizable polymer in the blend, c ($c \leqslant c' \leqslant 1$). If the nucleation rate is calculated per unit volume of crystallizable component, the nucleation constant I_0 should be used instead of I_{0b}. In equation (5), $T_{\infty b} = T_{gb} - 51.6\,\text{K}$, where T_{gb} is the glass transition temperature of the blend; and $\Delta g' = \Delta g_f + \Delta g_b$ is the free enthalpy of fusion in the mixture (Δg_f is the free enthalpy of melting of the crystal phase and Δg_b is the free enthalpy of mixing of blend components, both calculated per unit volume of crystallizing component in the blend).

In the proposed equation (5) the concentration of crystallizing polymer, c, does not appear explicitly. Instead there is the c' parameter depending on c. The reason for this is that the nucleation events occur preferably in a place where the local concentration of crystallizing segments c' fluctuates to values larger than the macroscopic concentration c. Some confirmation of such a concept is given by the investigation of crystallization of linear polyethylene from solution[13], which has shown that in the case of secondary nucleation $c' \sim c^{1/3}$. One can expect that a similar relation might be observed for primary nucleation in multicomponent systems.

The first exponential term in equation (5) describes the temperature dependence of the transport process. The transport of the segments that will be attached next to the forming nucleus proceeds in some limited surroundings of that nucleus. The size of such surroundings is at least of the order of the dimensions of a random coil, i.e. significantly larger than the nucleus size. Its volume is occupied by segments of several macromolecules of both components of the blend, although, as was stated above, the region is probably richer in crystallizable component (concentration c') than the blend (concentration c). Nevertheless, the transport process should be still considered as transport proceeding in the blend, not in plain crystallizing polymer. Thus, in equation (5) we introduced the parameter $T_{\infty b}$ (dependent on the glass transition temperature of the blend, T_{gb}) instead of T_∞, which is proper for plain polymer. Because both parameters, T_{gb} and $T_{\infty b}$, depend on composition, the $T_{\infty b}$ used in the equation should refer to the concentration c' rather than c. However, the local concentration c' may be different

for each nucleus, and in general its value is unknown and difficult to estimate. We propose to use the values of T_{gb} and $T_{\infty b}$ connected with the macroscopic concentration c instead of local concentration c'. The error introduced in this way into the calculation should be very small. In the case of blends of isomers (as in reported study), T_g practically does not depend on the composition in such systems, so $T_\infty = T_{\infty b}(c) = T_{\infty b}(c')$.

The free enthalpy $\Delta g'$ instead of Δg_f appears on the last term of equation (5). It takes into account the necessity of local separation of blend components during formation of a stable nucleus. The blend components are compatible in the molten state, thus $\Delta g_b < 0$, so the free enthalpy of separation $\Delta g_s = -\Delta g_b$ is greater than 0, i.e. the separation requires work. Since $\Delta g_f > 0$, hence $\Delta g' = (\Delta g_f + \Delta g_b) < \Delta g_f$, and therefore the energy barrier of a stable nucleus in a blend of compatible polymers is greater than in plain polymer. This results in the decrease of nucleation rate in the blend compared to that in plain polymer.

An additional assumption is made in the proposed equation: the surface energies of the crystal growing in the blend, σ and σ_e, do not depend on the blend composition and are equal to those in plain polymer. In the blends the values of σ and σ_e are most probably close to their respective values in plain polymer because they are mainly the result of surface ordering of the crystal rather than the crystal environment. In the case of a blend of isomers the above assumption is, in our opinion, justified.

Based on a similar consideration one can also describe the growth rate of spherulites growing from the melt of compatible polymers by the following equation (written for regime III crystallization):

$$G = G_{0b} \exp\left(-\frac{U^*}{R(T - T_{\infty b})}\right) \exp\left(-\frac{4b_0\sigma\sigma_e}{\Delta g' kT}\right) \quad (6)$$

in which $G_{0b} = c' G_0$ and $\Delta g' = \Delta g_f + \Delta g_b$.

The analysis of equations (5) and (6) shows that in blends of compatible polymers both primary and secondary nucleation (which controls the spherulite growth rate) should be depressed in comparison to a plain polymer because of significant increase in energy barrier of stable nucleus formation, connected with the phase separation phenomena.

Small-angle light scattering by impinged truncated spherulites

Small-angle light scattering (SALS) appeared to be a valuable technique for examining certain features of spherulitic polymers. It has been shown theoretically and demonstrated experimentally that the H_V SALS patterns (crossed polars) from unoriented spherulitic polymer film have the four-leaf clover appearance, with the scattering intensity showing a maximum at an azimuthal angle $\mu = 45°$ and at polar scattering angle θ dependent on the size of the spherulites[14,15]. The angle θ_m, at maximum scattering intensity, can be used for determination of the size of spherulites.

The first theoretical description of the light scattering pattern of spherulites was proposed by Stein and Rhodes[14]. They based their work on the model of a single spherulite as a homogeneous sphere with anisotropy of radial and tangential refractive indices, embedded in a homogeneous isotropic medium. They used the Rayleigh–Gans–Debye (RGD) approximation and developed from the RGD integral the expressions for intensity of scattered light. For H_V geometry they obtained the following equation:

$$I_{Hv} = C \cos^2 \rho_2 (R^3/U^3)^2 \{(\alpha_r - \alpha_t)[\cos^2(\theta/2)/\cos\theta] \times \sin\mu \cos\mu\,[4 \sin U - U \cos U - 3\,\mathrm{Si}(U)]\}^2 \quad (7)$$

where C is a constant, α_r and α_t are the radial and tangential polarizabilities of scattering elements within a spherulite, μ and θ are the azimuthal and polar scattering angles, $\cos\rho_2 = \cos\theta/(\cos^2\theta + \sin^2\theta \sin^2\mu)^{1/2}$, $U = (4\pi/\lambda)R \sin(\theta/2)$ and:

$$\mathrm{Si}(U) = \int_0^U [(\sin x)/x]\,dx.$$

Recently Champion, Killey and Meeten[16], using the identical spherulite model and the RGD approximation, derived the spherulite scattering matrix $\boldsymbol{S}$, on the basis of which they calculated the expressions for the intensity of light scattered by spherulites, which are more general than those obtained by Stein and Rhodes. For H_V geometry they obtained:

$$I_{Hv} = C(R^3/U^3)^2 \{2(\bar{m} - 1)\sin^2(\theta/2)(\sin U - U\cos U) - \tfrac{1}{3}\Delta m[2 + \cos^2(\theta/2)] \times [4 \sin U - U \cos U - 3\,\mathrm{Si}(U)]\}^2 \sin^2\mu \cos^2\mu \quad (8)$$

where $\bar{m} = (n_r + 2n_t)/(3n_s) = \bar{n}/n_s$ and $\Delta m = (n_r - n_t)/n_s$. The other symbols are the same as in equation (7). The quantities Δm and $\bar{m}$ are the anisotropy and the mean of the refractive index of the spherulite relative to that of the surrounding material (n_s), respectively.

At small scattering angles θ the first term of equation (8) is negligibly small compared with the second, provided that Δm is similar in magnitude to or larger than $(\bar{m} - 1)$. Under these conditions equation (8) reduces to a form equivalent to equation (7), so the Stein–Rhodes expression is wholly adequate. However, equation (8) is a better approximation if $\bar{m} - 1 \neq 0$ and θ is larger, and if a spherulite is weakly anisotropic or has a large mismatch with its surroundings[16].

Although the theoretical equations based on the model of perfect spherulites[14–16] predict well many of the features of SALS patterns, the experimentally measured scattering intensities, especially for samples filled completely with spherulites, were found to differ in detail from those calculated (see e.g. ref. 17). The experimentally measured intensity is lower at the maximum and higher at both smaller and larger angles than that predicted. Moreover, theory predicts zero scattering intensity at $\theta = 0°$ as well as at $\mu = 0°$ and 90°, whereas a finite scattering intensity is experimentally observed. These discrepancies between theory and experimental results are attributed to the internal and external disorder of spherulites within a polymer sample[17]. In addition, other various experimental factors (such as refraction at sample interfaces and multiple scattering of light inside the volume of the sample) produce deviations from the predicted intensity profile.

The influence of internal disorder on the H_V SALS pattern is described well by the Yoon–Stein theory of orientational disorder[18]. The internal disorder lowers the scattering intensity at the maximum and increases it at larger and smaller scattering angles, giving the finite scattering at $\theta = 0°$.

The external disorder includes incomplete spherulite

development, interspherulitic interference, distribution of spherulite sizes and their truncation due to impingement of neighbouring spherulites during their growth.

The effect of interspherulitic interference gives rise to the sinusoidal modulation of the scattering profile[19]. Such modulation produces some coarseness of the scattering pattern and can be neglected if the sample contains a larger number of scattering spherulites.

The distribution of spherulite sizes leads to the lowering and broadening of the scattering intensity maximum, and so does the truncation of spherulites[20–23]. The broadening of scattering profile caused by the truncation of spherulites is much more distinct than that due to size distribution and gives rise to finite scattering at $\theta=0°$ as well as at $\mu=0°$ and $\mu=90°$[22,23]. Moreover, the effects of truncation and spherulite size distribution together change the meaning of an average spherulite radius as determined from SALS. The SALS-determined average radius appears to be heavily weighted in favour of larger spherulites[21–23]. Tabar *et al.*[22,23] have found that the average spherulite radius determined from SALS is the quotient of averages of n and $(n-1)$ order, where n varies in the range 4–6 depending on the dimensionality of the spherulites and the mode of primary nucleation.

We have attempted to describe the SALS by an assembly of impinged truncated spherulites using a mathematical description of the spherulitic structure. For that, we have utilized the description of spherulitic structure developed recently in our laboratory based on statistical mathematics[24].

Although the expression for I_{Hv} obtained by Champion *et al.*[16] on the basis of another approach is more general than that proposed by Stein and Rhodes[14], we have used the Stein–Rhodes method to derive the equation for H_v intensity. The Stein–Rhodes treatment seems to be a sufficiently good approximation in the case considered here of a spherulite surrounded by other spherulites with identical optical properties (i.e. sample filled completely with spherulites). The refractive index of the surrounding medium, n_s, is very close to the average index of a single spherulite, $\bar{n}$. In such a case $|\bar{m}-1|$ is expected to be of the order of 10^{-3} or smaller[14,25], hence, most frequently smaller than the anisotropy of spherulites, Δn. If the condition $|\bar{m}-1| \leqslant \Delta m$ is satisfied, for small scattering angles both Stein–Rhodes and Champion *et al.* equations for I_{Hv} are equivalent (see discussion of equation (8)). The above condition is valid also for the model proposed here. However, the model is applicable only to those polymeric systems in which the spherulites have an anisotropy at least of the order 10^{-3}.

Statistical description of spherulite boundaries. The spherulite size distribution and spherulite truncation are readily considered within a statistical description of spherulite structure, in particular in the equations describing the distribution of distances between the spherulite centres and their boundary points. Such a distribution defines the probability $p(r)$ of finding within a sample filled completely with spherulites a point belonging to the interspherulitic boundary at distance r from the centre of a spherulite. All boundary points of all spherulites in the sample are represented in that distribution. The positions of boundary points are fully determined by the effects of impingement of neighbouring spherulites during their growth, so that the distance distribution of boundary points consists of overall information concerning both spherulite size distribution and truncation of spherulites in the spherulitic sample.

The distance distributions for cases of two- and three-dimensional spherulitic structures as well as different modes of primary nucleation (instantaneous, sporadic and mixed) are described by the following equations[24].

(i) Instantaneous nucleation (in normalized form):

$$p^2(r)=4\pi D^{3/2} r^2 \exp(-\pi D r^2) \tag{9a}$$

$$p^3(r)=\tfrac{9}{2}(\tfrac{4}{3}\pi D)^{4/3}\frac{r^4}{\Gamma(2/3)}\exp(-\tfrac{4}{3}\pi D r^3) \tag{10a}$$

where D is the density of instantaneous nucleation (i.e. number of instantaneous nuclei per unit volume) and $\Gamma(x)$ is the gamma function.

(ii) Sporadic nucleation (in normalized form):

$$p^2(r)=3\left(\frac{\pi J}{3G}\right)^{2/3}\frac{r}{\Gamma(2/3)}\exp\left(-\frac{\pi J r^3}{3G}\right) \tag{9b}$$

$$p^3(r)=4\left(\frac{\pi J}{3G}\right)^{3/4}\frac{r^2}{\Gamma(3/4)}\exp\left(-\frac{\pi J r^4}{3G}\right) \tag{10b}$$

where J is the rate of sporadic nucleation (number of sporadic nucleation events per unit volume per unit time) and G is the spherulite growth rate.

(iii) Mixed nucleation (in unnormalized form):

$$p^2(r)=2\pi r\left(2\pi D^2 r+\pi D\frac{J}{G}r^2+\frac{J}{G}\right)\exp\left[-\pi r^2\left(D+\frac{rJ}{3G}\right)\right] \tag{9c}$$

$$p^3(r)=4\pi r^2\left(4\pi D^2 r^2+4\pi\frac{DJ}{3G}r^3+\frac{J}{G}\right)\times\exp\left[-\tfrac{4}{3}\pi r^3\left(D+\frac{rJ}{4G}\right)\right] \tag{10c}$$

The formulae (9a)–(9c) describe the distribution for the case of two-dimensional spherulitic structures, whereas formulae (10a)–(10c) are for three-dimensional structures, respectively.

Using the normalized form of appropriate distribution of distances of boundary points to the spherulite centres, one can define an nth-order average spherulite radius of the assembly of spherulites:

$$\langle R_n\rangle=\frac{\langle R^n\rangle}{\langle R^{n-1}\rangle}=\frac{\int_0^\infty r^n p(r)\,\mathrm{d}r}{\int_0^\infty r^{n-1}p(r)\,\mathrm{d}r} \tag{11}$$

where $n\geqslant 1$ denotes the order of averaging. The definition of the average radius given by equation (11) is a continuous analogue of the discrete definition proposed by Tabar *et al.*[22,23].

Light scattering. In the Rayleigh–Gans–Debye approximation the amplitude of light scattered by an anisotropic system is given by the equation:

$$E_x=C\int_V (\boldsymbol{M}\cdot\boldsymbol{O})_x \exp[\mathrm{i}k(\boldsymbol{r}\cdot\boldsymbol{s})]\,\mathrm{d}^3\boldsymbol{r} \tag{12}$$

where C is a constant; $\boldsymbol{M}$ is the induced dipole moment in the scattering element whose position is determined by the vector $\boldsymbol{r}$; $\boldsymbol{O}$ is the unit vector perpendicular to the scattered ray and in the plane of polarization of the light transmitted by the analyser; $k=2\pi/\lambda$ is the wavenumber (λ is the wavelength in the medium) $\boldsymbol{s}=\boldsymbol{s}_0-\boldsymbol{s}_1$ denotes

the propagation vector (s_0 and s_1 are unit vectors parallel to the incident and scattered beams); and d^3r is the differential volume element. The subscript x refers to the particular orientation of polarizer and analyser.

In early models the integration was conducted over the volume of a single spherulite; hence those models do not take into consideration the effects of either spherulite size distribution or spherulite truncation in the polymer sample.

In order to consider those effects we introduce here the concept of a representative of the sample 'mean' spherulite. The basic idea of the proposed approach is to substitute the assembly of size-distributed and truncated real spherulites (generally not centrosymmetric in shape) completely filling the volume of sample by a single centrosymmetric model spherulite built from anisotropic elements having radial and tangential polarizabilities identical to the elements within the real spherulites (similar to Stein's model of perfect spherulite[14,15]). The most important feature of this new object is that it has infinite dimensions, and that the amplitude of light scattered by any element is modified by the weight dependent on the position of that element within the model spherulite. The weight for scattering is determined by the probability $p(\boldsymbol{R})$ that in particular direction $\boldsymbol{R}$ in the sample one finds an interspherulitic boundary located at distance $|\boldsymbol{R}|$ from the centre of a spherulite. Such a probability can be approximated by the normalized distance distribution of boundary points, $p(R)$, presented in the previous section. As was mentioned earlier, the distribution $p(R)$ includes the overall information on size distribution and truncation of spherulites averaged over all directions and all spherulites within this sample. Owing to the weighting procedure, that information will be transferred to the calculated scattering pattern. One must remark, however, that the probability given by the distance distribution depends only on the distance R from the spherulite centre and not on the direction within the sample. Also the scattering by a real sample is produced by a limited number of neighbouring spherulites, not by the infinite sample as in the statistical description. As a consequence, the proposed approach will not predict satisfactorily all the details of the scattering profile.

We propose the following equation for the H_V amplitude of scattered light produced by a representative 'mean' spherulite (three-dimensional case):

$$E^3_{H_V} = c \int_{R=0}^{\infty} p^3(R) \left(\int_{r=0}^{R} \int_{\alpha=0}^{\pi} \int_{\phi=0}^{2\pi} (\boldsymbol{M}\cdot\boldsymbol{O})_{H_V} \times \exp[ik(\boldsymbol{r}\cdot\boldsymbol{s})] r^2 \sin\alpha \, d\alpha \, d\phi \, dr \right) dR \qquad (13a)$$

The three internal integrals over ϕ, α and r, respectively, represent the scattering by a single ideal spherulite having radius R as derived by Stein and Rhodes[14]. Thus:

$$E^3_{H_V} = \int_0^{\infty} p^3(R) E_{single}(R) \, dR$$
$$= C(\alpha_r - \alpha_t) \cos\rho_2 \sin\mu \cos\mu \, [\cos^2(\theta/2)/\cos\theta] \times \int_0^{\infty} p^3(R)(R^3/U^3)[4\sin U - U\cos U - 3\,\mathrm{Si}(U)] \, dR \qquad (13b)$$

where k is a constant and the other symbols are the same as in equation (7).

However, in equation (13) the interpretation of R is different than in Stein's model. The radius R now describes the sequence of scattering elements in the model 'mean' spherulite starting from its centre and ending at the distance R, and to which the weight $p^3(R)$ is ascribed.

The model has a flaw because the representative 'mean' spherulite is centrosymmetric while truncated spherulites show in general a lack of a centre of symmetry. It was shown[23] that lack of a centre of symmetry in truncated spherulites leads to finite scattering at $\theta = 0°$, but otherwise does not change the scattering pattern. Our model predicts zero scattering intensity at that angle, similarly to the perfect spherulite model[14,15]. For the same reason the intensity profile along azimuthal angle μ has for the proposed model a shape similar to the profile resulting from the perfect spherulite model, with zero intensity at $\mu = 0°$ and 90°. The scattering patterns of non-centrosymmetric structures, such as truncated spherulites, have a different profile along μ—broader and with finite scattering intensity at $\mu = 0°$ and 90°[22,23].

The main advantages of the proposed model are the relative simplicity of the calculations and the possibility of the correlation of the intensity profile directly with the parameters of primary nucleation and growth of spherulites. These parameters, which determine the shape of the spherulitic structure, are present in the distribution $p(R)$.

Typical calculated intensity profiles are depicted in *Figures 1a* and *1b* for two- and three-dimensional cases, respectively. The intensity curves for a single non-truncated spherulite calculated using Stein's model are also plotted for comparison in those figures. It is seen that, in all considered cases of dimensionality of the system as well as nucleation modes, the profiles of intensity of H_V light scattering differ markedly from those calculated for perfect single spherulites with equal dimensions ($R_{single} = \langle R \rangle$). One of the differences is that for our model the higher-order peaks are not present in the scattering intensity curve. Instead the first-order peak has a tail at higher values of reduced variables $w = (2\pi/\lambda)\langle R \rangle \sin\theta$ (two-dimensional case) and $U = (4\pi/\lambda)\langle R \rangle \sin(\theta/2)$ (three-dimensional case). Another, most important, difference is that the positions of the maxima of scattered light intensity in the presented model are located at lower values of w and U than the position of the first-order maximum for the respective perfect spherulite. This leads to the conclusion that the number-average spherulite radius $\langle R \rangle$ is not an adequate parameter for the purposes of light scattering.

Our calculations show that for two- and three-dimensional spherulite structures the average radii $\langle R_4 \rangle = \langle R^4 \rangle / \langle R^3 \rangle$ (as defined by equation (9)) and $\langle R_5 \rangle = \langle R^5 \rangle / \langle R^4 \rangle$ should be used, respectively. An illustration of the above is given in *Figures 2a* and *2b*, in which the intensity profiles as in *Figure 1* are replotted against reduced variables $w_4 = (2\pi/\lambda)\langle R_4 \rangle \sin\theta$ (two-dimensional case, *Figure 2a*) and $U_5 = (4\pi/\lambda)\langle R_5 \rangle \sin(\theta/2)$ (three-dimensional case, *Figure 2b*). It is seen that the maxima predicted by our model and by the perfect spherulite model coincide at the same value of reduced variables: $w_4 = 3.9$ (two dimensions) and $U_5 = 4.1$ (three dimensions). Such coincidence takes place independently of the values of nucleation parameters used for calculations (i.e. of size of spherulites). Moreover, the calculations show that the shape of the intensity curve plotted *versus* w_4 or U_5, respectively (for a given dimensionality), depends very

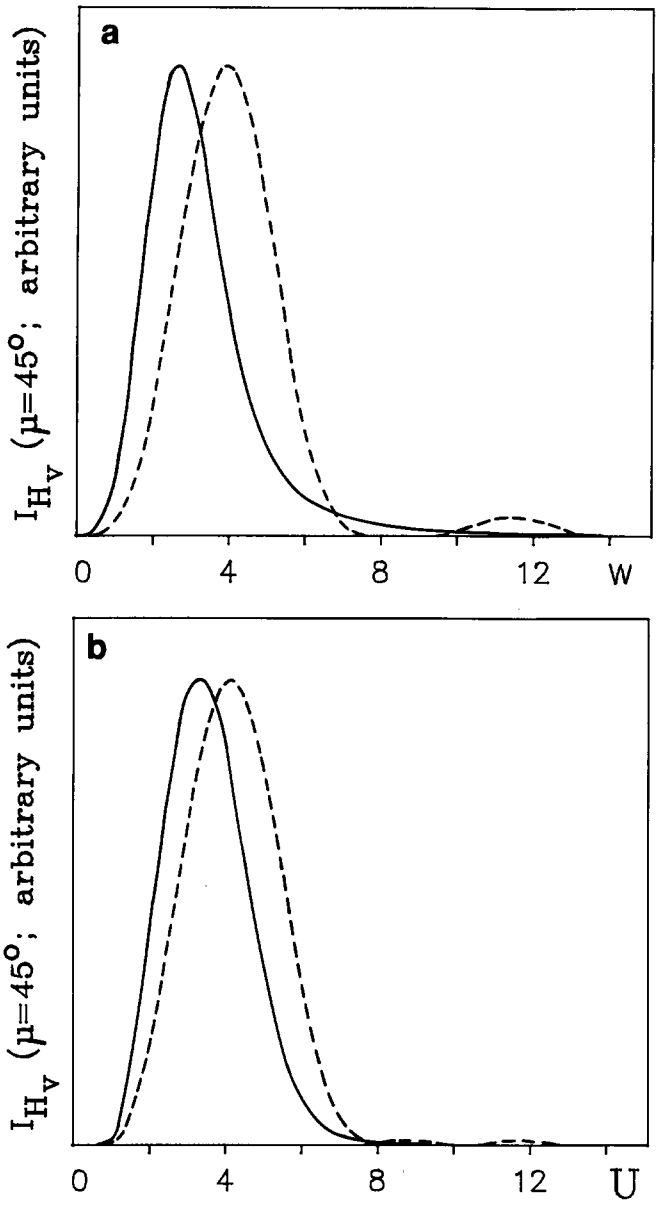

Figure 1 Typical H_V SALS intensity profiles at $\mu=45°$ calculated using the proposed model (full curve), plotted against the reduced variables (a) $w=(2\pi/\lambda)\langle R\rangle \sin\theta$ (two-dimensional case) and (b) $U=(4\pi/\lambda)\langle R\rangle \sin(\theta/2)$ (three-dimensional case), where R is an average spherulite radius. The profiles calculated according to the perfect spherulite model for spherulites with radius $R=\langle R\rangle$ are also shown (broken curves). (a) Two-dimensional spherulitic structure: values of $D=10^6$ nuclei/cm^2, $I=2\times10^6$ nuclei/cm^2 s, $G=1\,\mu m\,s^{-1}$ and $R=2.28\,\mu m$ were assumed for calculations. (b) Three-dimensional spherulitic structure: values of $D=10^{10}$ nuclei/cm^3, $I=10^{10}$ nuclei/cm^3 s, $G=1\,\mu m\,s^{-1}$ and $R=2.38\,\mu m$ were assumed

little on the mode of nucleation and on the values of nucleation parameters (in the range studied).

On the basis of the above considerations, one can conclude that the average spherulite radius determined by the SALS measurements is not the number-average but the nth-order average spherulite radius $\langle R_n\rangle$. The value of n depends only on the dimensionality of the spherulite structure: $n=4$ for assemblies of two-dimensional spherulites and $n=5$ for assemblies of three-dimensional spherulites. Such a conclusion is in good agreement with that drawn previously by Tabar *et al.*[22,23] on the basis of computer simulation.

The average radii $\langle R_n\rangle$ ($n=4$ or 5) can be determined directly from the angle of maximum scattering intensity using formulae similar to those known from perfect spherulite models:

two-dimensional case

$$\langle R_4\rangle=\frac{3.9\lambda}{2\pi\sin(\theta_{max})} \tag{14a}$$

three-dimensional case

$$\langle R_5\rangle=\frac{4.1\lambda}{4\pi\sin(\theta_{max}/2)} \tag{14b}$$

Although the average radii $\langle R_4\rangle$ and $\langle R_5\rangle$, appropriate for dimensionality of the sample, are independent of the type of nucleation, the number-average radius $\langle R\rangle$ depends on it. Thus, the ratio $\langle R_n\rangle/\langle R\rangle$ depends on the

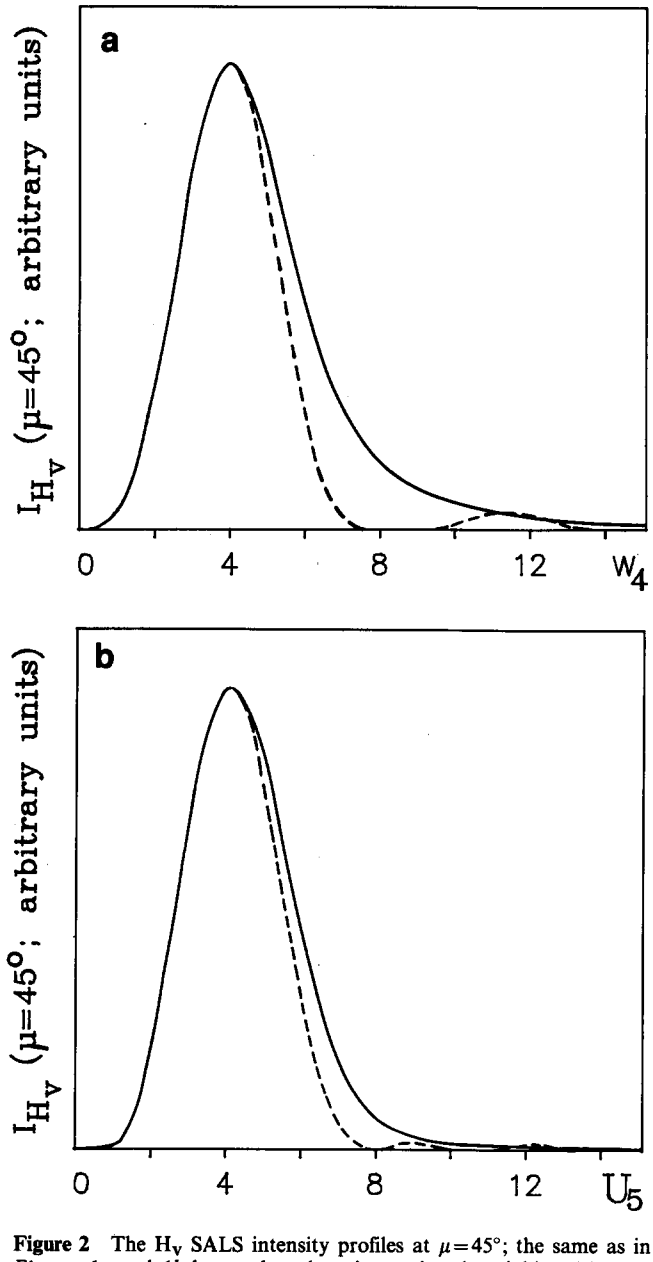

Figure 2 The H_V SALS intensity profiles at $\mu=45°$; the same as in *Figures 1a* and *1b* but replotted against reduced variables: (a) $w_4=(2\pi/\lambda)\langle R_4\rangle \sin\theta$, two-dimensional structure; (b) $U_5=(4\pi/\lambda)\langle R_5\rangle \sin(\theta/2)$, three-dimensional structure. The profiles calculated according to the perfect spherulite model for spherulites with radius $R=\langle R_4\rangle$ (two dimensions) and $R=\langle R_5\rangle$ (three dimensions) are also shown (broken curves)

type of nucleation or on the ratio of instantaneous to sporadic nuclei numbers in the case of mixed type of nucleation. The range of this variation is 1.47–1.50 for two-dimensional systems and 1.25–1.33 for three-dimensional systems, respectively. The limits of the variation are given by the values for pure instantaneous and sporadic nucleation modes. Only in such extreme cases can one determine precisely from the SALS data both $\langle R_n \rangle$ and $\langle R \rangle$ average radii. In the case of mixed nucleation, if the fractions of sporadic and instantaneous nuclei are unknown, the average radius $\langle R_n \rangle$ can be determined precisely but the radius $\langle R \rangle$ can only be estimated because the ratio $\langle R \rangle / \langle R_n \rangle$ depends on the ratio of sporadic to instantaneous nuclei numbers.

In the proposed model the H_V scattering pattern is fully determined by the parameters of primary nucleation and growth rate of spherulites, which control the shape of the spherulitic structure within the sample and hence also the distribution $p(R)$. Because the position of the maximum of scattering intensity in H_V pattern depends on primary nucleation parameters, it is possible to estimate them on the basis of the SALS data.

Determination of primary nucleation by SALS measurements

The truly instantaneous or truly sporadic (with single nucleation rate) modes of nucleation are observed experimentally very rarely. In most cases of polymeric materials and crystallization conditions, the nucleation process can be approximated with a mixed mode.

The boundary points distribution $p(r)$ for mixed nucleation mode in a three-dimensional sample is given by equation (8c). It depends on density D of instantaneous nuclei, sporadic nucleation rate J and spherulite growth rate G.

The average spherulite radius $\langle R_5 \rangle$, defined by equation (9), in such a case is also a function of those three parameters: $\langle R_5 \rangle = f(D, J, G)$. However, the sporadic nucleation rate J and the spherulite growth rate G appear in equation (8c) always as a ratio J/G. Thus, the number of independent variables reduces to two: D and J/G. It follows then that at least two independent experimental values of $\langle R_5 \rangle$ are needed for a successful application of the SALS technique to the study of primary nucleation. We suggest the 'best fit' of $\langle R_5 \rangle$ over the temperature range of crystallization as a more precise solution.

All primary nuclei formed during polymer crystallization can be classified into three types: homogeneous, heterogeneous and self-seeded. The theory predicts that homogeneous nucleation is sporadic (with constant rate dependent on temperature of crystallization), whereas heterogeneous and self-seeding nucleations may exhibit more complicated behaviour (see e.g. ref. 11). The heterogeneous nuclei can appear as sporadic (with some spectrum of nucleation rates) or instantaneous, dependent on the type of heterogeneities inducing the nucleation (the substrates) as well as their surface geometry. The self-seeding nucleation behaves similarly. Experimental observations show that at low and intermediate supercoolings the heterogeneous and self-seeded nuclei are most frequently instantaneous or almost instantaneous (with some induction time)[11]. Detailed study of nucleation in poly(3-hydroxybutyrate) (PHB)[26] showed, however, that all nucleation types are in fact sporadic, although the heterogeneous and self-seeding nucleations have much higher nucleation rates than homogeneous nucleation; for example heterogeneous nuclei formed on saccharin crystals have nucleation rate approximately 2–3 orders of magnitude higher than homogeneous nuclei formed at the same temperature. One can expect that for other nucleants and/or polymers such differences may be even higher. As a result, the heterogeneous nuclei are frequently observed as instantaneous.

Another property of the heterogeneous and self-seeded nuclei is that their number is limited in a given sample independently of crystallization conditions. The population of these nuclei is limited to the number of heterogeneities present in the volume of the sample as well as the number of sites in which the pre-existing crystal ordering was not completely destroyed during the melting and melt-annealing prior to crystallization.

Taking the above into consideration, one can assume that during crystallization proceeding at very high supercooling the homogeneous nucleation is sporadic in time, whereas the heterogeneous and self-seeding nucleations are instantaneous (a few or more orders of magnitude difference in the rates of homogeneous and heterogeneous nucleations is in our opinion sufficient support to make the above assumption here). Moreover, for sufficiently high supercooling, the number of heterogeneous and self-seeded nuclei in a given sample is constant because of the saturation effect—all potential nuclei are active. On the other hand, the homogeneous nucleation rate depends only on the crystallization temperature. The final number of nuclei of this type depends only on time from start to completion of crystallization.

Summarizing, the assumptions made here mean that the sporadic nucleation rate J in equations (9) and (10) can be substituted by the homogeneous nucleation rate I, alone, expressed by equations (3) and (5) for a plain polymer or blend, respectively. The density D of instantaneous nucleation can be approximated by the sum of the numbers (per unit volume) of heterogeneous and self-seeded nuclei active for given melting and crystallization conditions. If the melt-annealing temperature and time prior to crystallization are sufficiently high, all self-seeded nuclei are destroyed, and thus D is represented only by the density of heterogeneous nucleation.

It follows from equations (3), (4), (5) and (6) that, in plain polymer:

$$\frac{J}{G} = \frac{I}{G} = \frac{I_0}{G_0} \frac{\exp[-32\sigma^2\sigma_e/(\Delta g_f)^2 kT]}{\exp(-4b_0\sigma\sigma_e/\Delta g_f kT)} \tag{15}$$

and in a compatible blend:

$$\frac{J}{G} = \frac{I}{G} = \frac{I_0}{G_0} \frac{\exp[-32\sigma^2\sigma_e/(\Delta g')^2 kT]}{\exp(-4b_0\sigma\sigma_e/\Delta g' kT)} \tag{16}$$

It is apparent that J/G does not depend on the transport properties in a material and depends only on the energetic conditions of formation of stable primary and secondary nuclei. On the basis of the above equations and equations (10c) (the case of mixed nucleation; normalized) and (11), it is possible to calculate a theoretical dependence of fifth-order average spherulite radius $\langle R_5 \rangle$ on crystallization temperature for plain polymer and for the blend. The unknown parameters of the equation describing the case of plain polymer are now D and I_0 (both independent of temperature) instead of D, $I(T)$ and $G(T)$. All other parameters, i.e. σ, σ_e, T_m°, Δg_f, G_0 and b_0, are known or could be determined on the basis of separate experiments.

For the blend, the unknowns are D and I_0 (I_0 is the same as for plain polymer) and additionally the free enthalpy of mixing of blend components Δg_b. Assuming different values of these parameters, the calculated curve $\langle R_5 \rangle$ vs. T can be fitted to the curve obtained experimentally. As a result of such a procedure, the 'best-fit' values of nucleation constants D (heterogeneous and self-seeding nucleation density), I_0 (homogeneous nucleation rate constant) and Δg_b (free enthalpy of mixing of components in the blends) can be determined.

EXPERIMENTAL

The materials used in this study were: isotactic polypropylene, iPP (RAPRA, iPP1, $M_w = 3.07 \times 10^5$, $M_n = 1.56 \times 10^4$, $\rho = 0.906\ g\ cm^{-3}$, melt flow index = 3.9 g/10 min), and atactic polypropylene, aPP (Polish product, $M_w = 2.4 \times 10^4$, $\rho = 0.855\ g\ cm^{-3}$).

Before blending, the atactic n-heptane-soluble fraction was removed from commercial iPP by extraction. Blends of iPP (purified in such a way) with aPP, containing 0, 10, 20 and 30 wt% of aPP, were prepared by dissolving both polymers in the desired proportion in boiling xylene, followed by precipitation with excess methanol. The powders obtained were washed with acetone and dried under vacuum. The powders were then compression moulded into 40 μm thick foils in a laboratory press ($P = 50$ atm, $T = 220$°C, $t = 10$ min). After compression moulding the foils were quickly cooled down using liquid nitrogen in order to minimize the phase separation induced by crystallization. Samples in the form of circles 5 mm in diameter were cut out from the foils. A set of samples with different composition was placed in an aluminium spacer 40 μm thick possessing circular holes—one hole for each composition—fitted for the samples and sandwiched between two thin (5 μm thick) aluminium foils. In order to reduce the effect of fluctuations in thermal treatment, at least three sandwiches were crystallized for each crystallization temperature studied. Before crystallization the samples were melted and melt-annealed at 190°C for 5 min in order to restore the homogeneity of the blend. Then they were quickly transferred to the special crystallization cell maintained at a constant temperature within the range +60 to +82°C. The temperature of the cell was controlled using an electronic control unit with accuracy of ±0.05°C. The crystallization cell comprised two opposing cylindrical aluminium blocks (15 cm in diameter, 10 cm high) equipped with electrical heaters and temperature sensors connected to the temperature control unit. The surfaces of the blocks contacting the samples were carefully polished in order to improve thermal contact. The blocks were pressed quickly and firmly against each other (the force was ~10 kg) immediately after placing the samples between them. Owing to the small heat capacity of the samples, the large heat capacity of the cell and precise control of its temperature, as well as very good thermal contact between the samples and the cell via thin soft aluminium covering foils, the sample could be cooled down very quickly. Isothermal conditions were reached within the sample volume in less than 0.5 s after transferring it to the cell, as independently measured by a copper–constantan thin thermocouple placed inside the sample. That time is more than one order of magnitude shorter than the time needed for complete crystallization of iPP at those temperatures, estimated on the basis of published data[11].

Samples crystallized at different temperatures were investigated using the small-angle light scattering (SALS) technique in order to determine the fifth-order average spherulite radius $\langle R_5 \rangle$ from the H_V scattering pattern. A He–Ne laser ($\lambda = 632.8$ nm) was used to generate the scattering patterns. The H_V scattering light intensity distribution along scattering angle θ was measured at fixed $\mu = 45°$ directly using the goniometer with photodetector connected to the recorder.

For each blend composition and crystallization temperature, three or more samples were studied. On the basis of the measured scattering angle of maximum intensity, θ_m, the values of $\langle R_5 \rangle$ for each sample were calculated using equation (14b). Then the mean values of $\langle R_5 \rangle$ were calculated for each blend composition and crystallization temperature. The absolute error of the values of average spherulite radii determined in that way did not exceed ±0.5 μm.

On the basis of the SALS-determined dependence of $\langle R_5 \rangle$ on the crystallization temperature, the instantaneous nucleation densities and the sporadic nucleation rates were estimated according to the procedure proposed in the previous section.

As was stated in the theoretical section, the justification for using a procedure based on the proposed model (similar to the use of Stein's equations for a single spherulite) is that the spherulite anisotropy relative to the surrounding material, Δm, is larger than $|\bar{m} - 1|$, i.e. it is of the order of 10^{-3} or larger.

We determined the value of Δm for iPP spherulites (grown from molten plain iPP or the mixture of iPP with aPP) on the basis of estimates from the literature data only, because direct measurements of spherulite anisotropy in the studied iPP and iPP/aPP samples, in which rather weakly anisotropic spherulites completely fill the sample volume and have sizes of only a few micrometres (i.e. much less than the sample thickness), are extremely uncertain. Spherulites in polypropylene crystallized below 137°C have anisotropy $\Delta n = (n_r - n_t)$ ranging from +0.001 to +0.004 (higher values are associated with lower crystallization temperatures)[27]. Because in the present study the crystallization of the samples was conducted at very low temperatures, the value close to 0.004 should be used for estimation of Δm. The average refractive index of polypropylene, n_s, ranges from 1.471 to 1.525 depending on the degree of crystallinity (from 0%, i.e. fully amorphous material, to 100%, respectively)[28]. Hence, $\Delta m \simeq 0.0026$–0.0027, which is larger than $\bar{m} - 1$ (postulated[25] to be equal to or less than 10^{-3}), which suggests the applicability of the procedure proposed in this paper for analysis of the SALS experimental data obtained for the studied iPP and iPP/aPP blend samples. On the other hand, taking $\Delta n = 0.001$, then Δm can be estimated as 0.000 66 only, i.e. the condition $\Delta m > \bar{m} - 1$ is not satisfied. Assuming this lower value of Δm and $\bar{m} - 1 = 0.001$ (upper limit for a spherulite surrounded by other identical spherulites, postulated in ref. 25), we have calculated the intensity of light scattered by a single spherulite, I_{HV}, using two equations, i.e. that given by Stein and Rhodes (equation (7)) and that given by Champion *et al.* (equation (8)). For those values of Δm and $(\bar{m} - 1)$, both equations predict practically the same profile of the intensity of scattered light with identical location of the maximum ($U = 4.1$). This shows that the Stein–Rhodes approach is still adequate even under the extreme conditions assumed here. This in turn

suggests the applicability of the procedure proposed in this paper to analyse the SALS experimental data obtained for iPP and iPP/aPP blend samples.

Some supplementary measurements of spherulite growth rate and melting temperature of iPP and iPP/aPP blends were performed. The radial growth rate of spherulites was determined using a light polarizing microscope equipped with a hot stage (the temperature of which was controlled with an accuracy of 0.1°C) and TV camera. For that purpose samples of blends placed on microscope slides and covered with cover glass were melt-annealed at 220°C, and then crystallized isothermally on the microscope hot stage at temperatures within the range 121–132°C. In appropriate time intervals the spherulite diameter was measured directly on the TV monitor and the growth rate was calculated.

In order to determine the melting behaviour, the iPP and the samples of blends were crystallized isothermally in a d.s.c. cell (Perkin–Elmer DSC 2B) at temperatures in the range 119–131°C. After completion of crystallization the samples were heated at 10°C min^{-1} in order to observe melting. The melting temperature of each sample was determined as the temperature of the maximum of the melting peak. On the basis of the observed melting temperatures as functions of crystallization temperature, the equilibrium melting temperature of iPP, T_m°, and its depression in the blends were calculated[11].

RESULTS AND DISCUSSION

Figure 3 shows the dependence of fifth-order average spherulite radius $\langle R_5 \rangle$ on the crystallization temperature for iPP and iPP/aPP blends, determined on the basis of SALS measurements. It is seen that for each composition the shapes of the curves are similar. On each of these curves three regions can be distinguished: for highest crystallization temperatures (smallest undercoolings, ΔT) all the curves are flat and $\langle R_5 \rangle$ is almost independent of T; for lower crystallization temperature (ΔT increased)

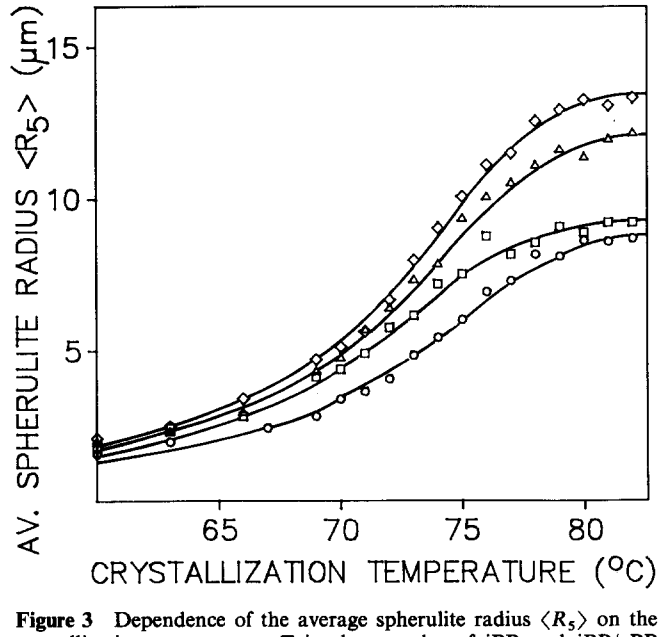

Figure 3 Dependence of the average spherulite radius $\langle R_5 \rangle$ on the crystallization temperature T in the samples of iPP and iPP/aPP blends: (○) iPP; (□) iPP/aPP, 9:1; (△) iPP/aPP, 8:2, (◇) iPP/aPP, 7:3. The full curves represent the 'best-fit' curves calculated for the nucleation parameters reported in *Table 2*

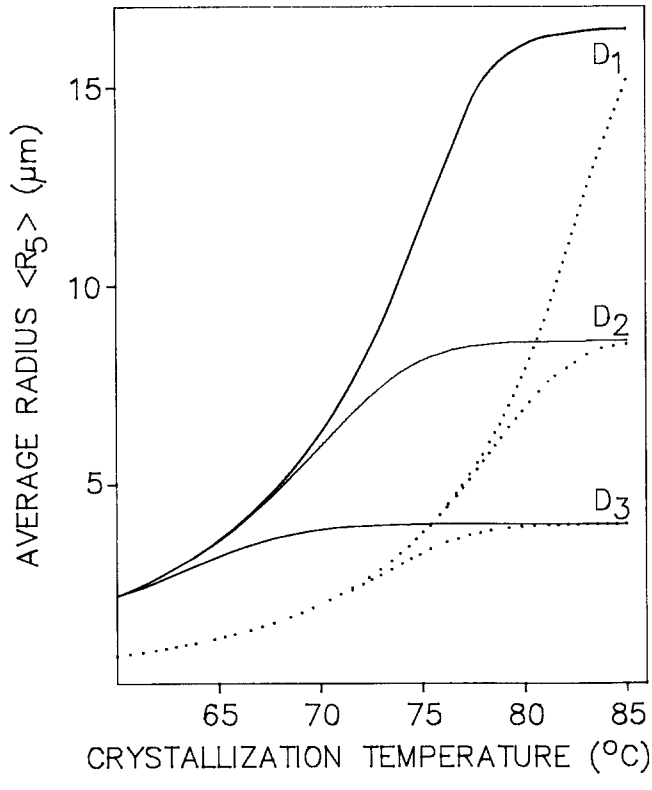

Figure 4 The model curves of the dependence of the average spherulite radius on the crystallization temperature. The curves were calculated from equations (8c), (9) and (13) assuming various values of instantaneous nucleation density D ($D_1 = 10^8$ nuclei/cm^3, $D_2 = 10^9$ nuclei/cm^3, $D_3 = 10^{10}$ nuclei/cm^3) and sporadic nucleation constant I_0 (full curves, 10^{35} nuclei/cm^3 s; broken curves, 10^{37} nuclei/cm^3 s)

$\langle R_5 \rangle$ depends strongly on temperature and decreases with the decrease of T; and for lowest crystallization temperatures the dependence of $\langle R_5 \rangle$ on T is again weak.

Figure 4 shows examples of model curves of $\langle R_5 \rangle$ vs. T calculated for various assumed values of the instantaneous nucleation D and the sporadic nucleation rate constant I_0, both independent of T. Other parameters used in the calculations were typical for isotactic polypropylene. The shapes of the model curves are similar to the shapes of the experimental ones. It is seen that for smallest undercooling the sporadic nucleation is weak, so the spherulite radius is controlled by the instantaneous nucleation (whose density is independent of temperature); thus the curve of $\langle R_5 \rangle$ vs. T is flat in that range of temperature. With increased undercooling, the number of sporadic nuclei increases markedly and finally becomes larger than the number of instantaneous nuclei. That results in a strong decrease of $\langle R_5 \rangle$. With further increase of undercooling, the rate of sporadic nucleation continuously increases, but the number of spherulites increases much more slowly because of the simultaneous decrease of time for spherulite nucleation and growth. As a result, the dependence of $\langle R_5 \rangle$ on T is not as strong as for intermediate undercoolings.

For fitting the calculated curves $\langle R_5 \rangle$ vs. T to the experimental data, it is necessary to know the following material constants for iPP: equilibrium melting temperature T_m°, enthalpy of fusion Δh_f, crystal surface energies σ and σ_e, spherulite growth rate constant G_0 and distance of fold planes b_0. All these data are known from published reports (see e.g. ref. 11). However, a large variety of values of T_m°, σ_e and G_0 for iPP exist in the literature. For this

reason we determined the values of those parameters for iPP used in this study on the basis of independent experiments.

The value of T_m° for iPP was determined from the dependence of melting temperature on the temperature of isothermal crystallization, presented in *Figure 5*. Additionally, the depression of the melting temperature in the blends was also determined. The results are presented in *Table 1*. The value of $T_m^\circ = 191°C$ determined was used in further calculations.

In *Figure 6* the measured growth rates of spherulites in plain iPP as well as in iPP/aPP blends are plotted against crystallization temperature. From *Figure 6* the values of σ_e and G_0 were calculated for plain iPP based on equation (4) in logarithmic form. Regime III crystallization and values of $U^* = 4120\,\text{cal mol}^{-1}$, $T_g = -12°C$, $\Delta h_f = 1.96 \times 10^9\,\text{erg cm}^{-3}$ and $\sigma = 11.5\,\text{erg cm}^{-3}$ were assumed[10,12]. Depending on the assumed fold plane, the following results were obtained:

(i) (1 1 0) fold plane ($b_0 = 6.26$ Å)

$$\sigma_e = 86.1\,\text{erg cm}^{-3}$$

$$G_0 = 1.17 \times 10^6\,\text{cm s}^{-1}$$

(ii) (0 4 0) fold plane ($b_0 = 5.24$ Å)

$$\sigma_e = 102.9\,\text{erg cm}^{-3}$$

$$G_0 = 1.17 \times 10^6\,\text{cm s}^{-1}$$

Both (i) and (ii) sets of b_0, σ_e and G_0 values were used in the calculations of theoretical dependences of $\langle R_5 \rangle$ on T from equations (10) (normalization performed), (11) and (15). Varying the values of the instantaneous (heterogeneous plus self-seeding) nucleation density D and the sporadic (homogeneous) nucleation rate constant I_0, the calculated curves were fitted to experimental data

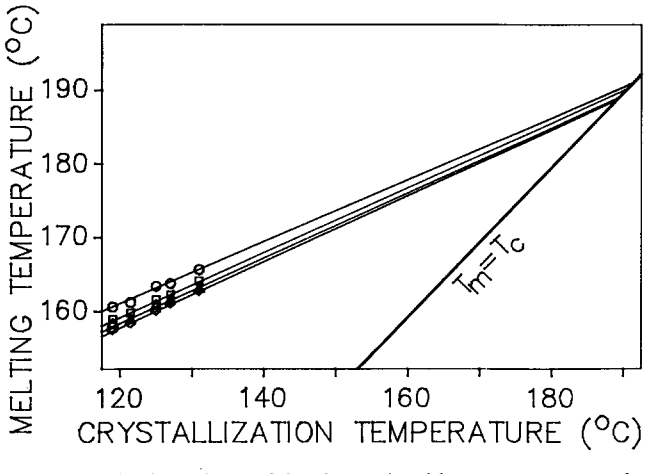

Figure 5 The dependence of the observed melting temperature on the temperatures of isothermal crystallization for iPP and iPP/aPP blends: (○) iPP; (□) iPP/aPP, 9:1; (△) iPP/aPP, 8:2; (◇) iPP/aPP, 7:3

Table 1 Equilibrium melting temperatures T_m° of iPP and its depression in the blends

Composition	T_m°, T_m (°C)	$\Delta T = T_m^\circ - T_m$ (°C)
iPP	191	0
iPP/aPP, 9:1	190.5	0.5
iPP/aPP, 8:2	189.4	1.6
iPP/aPP, 7:3	188.6	2.4

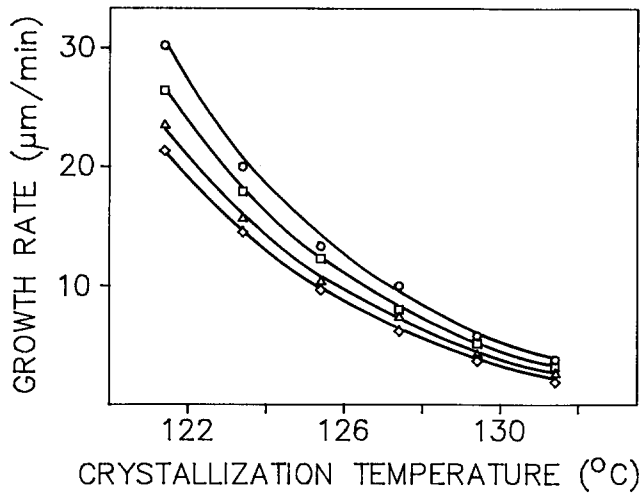

Figure 6 The dependence of the spherulite growth rate on the temperature of isothermal crystallization for iPP and iPP/aPP blends: (○) iPP; (□) iPP/aPP, 9:1; (△) iPP/aPP, 8:2; (◇) iPP/aPP, 7:3

Table 2 'Best-fit' values of athermal nucleation density D, homogeneous nucleation rate constant I_0 and free enthalpy of mixing Δg_b calculated for iPP/aPP blends

Composition	D (cm^{-3})	I_0 ($\text{cm}^{-3}\,\text{s}^{-1}$)	Δg_b (erg cm^{-3})
iPP	9.6×10^8	9.5×10^{35}	-
iPP/aPP, 9:1	7.0×10^8		-5.0×10^6
iPP/aPP, 8:2	4.0×10^8		-7.5×10^6
iPP/aPP, 7:3	2.8×10^8		-9.0×10^6

for iPP. Good fits were obtained when the (0 4 0) fold plane was assumed, whereas under the assumption of a (1 1 0) fold plane it was not possible to fit satisfactorily the calculated curves to the experimental data for any values of D and I_0. The possible cause of this is that at high undercooling polypropylene crystallizes according to regime III[12]. In this regime the chains may fold not only in the (1 1 0) plane (which is preferred in regime I) but frequently also in other than (1 1 0) planes, including the most probable (0 4 0) plane (see ref. 12). At high undercoolings the (0 4 0) plane may become a major plane of crystal growth.

The 'best fit' is achieved for $D = 9.6 \times 10^8$ nuclei/cm^3 and $I_0 = 9.5 \times 10^{35}$ nuclei/cm^3 s ((0 4 0) fold plane assumed in calculations of σ_e and G_0). The homogeneous nucleation rate constant I_0 is valid according to the proposed model for both plain iPP and its blends with aPP. Its value is close to that predicted by theory, i.e. 10^{34} nuclei/cm^3 s[10], and seems to be reliable. In previous investigations of homogeneous nucleation in plain polymers by the droplet technique[5–8], the estimated values of I_0 were several orders of magnitude higher.

Using determined homogeneous nucleation rate constant I_0, the fitting procedure was also performed for iPP/aPP blends. The 'best-fit' values of D, I_0 and Δg_m for iPP and iPP/aPP blends are summarized in *Table 2*. The data presented in this table show that the absolute value of the free enthalpy of mixing $|\Delta g_b|$ increases with increasing content of aPP in the blend, which is in accordance with the predictions[29].

In order to test the reliability of the determined parameters and the proposed approach to homogeneous nucleation in blends, the values of Δg_b were compared

with values of Δg_b estimated on the basis of the results of independent experiments. The free enthalpy of mixing was calculated from the depression of melting temperature in the blend, ΔT_m, using the following equation[30]:

$$\Delta g_b = -\Delta h_f(\Delta T_m / T_m^\circ)$$

The values of Δg_b were also estimated independently from spherulite growth rates in the iPP/aPP blends. Equation (6) was used in those calculations.

A comparison of the Δg_b values obtained from the procedure of nucleation-constant determination, melting-point depression and growth-rate depression is summarized in *Table 3*. It is seen that all three independent sets of Δg_b do not differ markedly. This indicates that the presented approach to homogeneous primary nucleation in blends is correct. Using the parameters I_0 and Δg_b reported in *Table 2*, the homogeneous nucleation rates I, calculated per unit volume of iPP present in the blend, as a function of crystallization temperature for different blend compositions were calculated from equation (5). The curves determined in this way are plotted in *Figure 7*. It is seen that at any fixed temperature of crystallization the rate of homogeneous nucleation decreases with increasing content of aPP in the blend. The cause of this decrease is the phase separation of blend components necessary for the formation of primary nuclei and growth of iPP crystal phase. The separation is connected with overcoming the additional energy barrier, which increases with the increase of the concentration of aPP in the blend. Moreover, the rate of homogeneous nucleation calculated per unit volume of the blend (not iPP in the blend, as above) is also lowered due to the decrease of the concentration of crystallizable macromolecules of iPP in the system.

Table 3 The free enthalpy of mixing Δg_b calculated per unit volume of iPP in the blend estimated on the basis of the measurements of nucleation constant, melting-point depression ΔT_m and spherulite growth rates G in the iPP/aPP blends

	$\Delta g_b \times 10^{-6}$ (erg cm^{-3}) estimated from measurements of		
Composition	ΔT_m	G	Primary nucleation
iPP/aPP, 9:1	−2.0	−2.0	−5.0
iPP/aPP, 8:2	−6.5	−4.0	−7.5
iPP/aPP, 7:3	−10.0	−5.0	−9.0

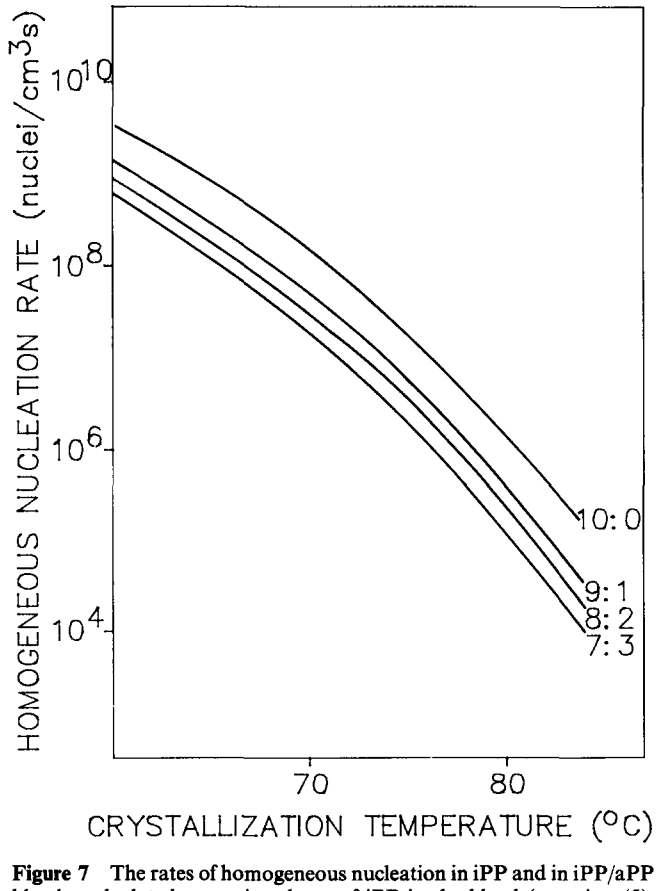

Figure 7 The rates of homogeneous nucleation in iPP and in iPP/aPP blends, calculated per unit volume of iPP in the blend (equation (5); I_0 and Δg_b taken from *Table 2*), plotted against crystallization temperature

The results presented in *Table 2* show also that the instantaneous nucleation, being the sum of heterogeneous and self-seeded primary nucleations, is depressed in the presence of aPP in the blend, although not as strongly as for homogeneous nucleation. However, the heterogeneous and self-seeding nucleations are not as sensitive as homogeneous nucleation to the changes in energy barrier for crystal nucleus formation[11]. In our opinion, the changes in the number of heterogeneous and self-seeded nuclei in the blends compared with plain iPP are induced mainly by the changes in concentration of crystallizing polymer in the blend.

CONCLUSIONS

On the basis of the results presented in this paper, the following conclusions can be drawn.

A method for studying homogeneous nucleation and other modes of primary nucleation of spherulites in plain polymers and in polymer blends crystallized in bulk was developed and tested.

An average spherulite radius $\langle R_5 \rangle$ in a polymer sample, which is an experimentally measured quantity, is determined by the total number of primary nuclei formed during crystallization and by the mode of primary nucleation. For higher crystallization temperatures, practically all nuclei are heterogeneous and self-seeded, so their number determines $\langle R_5 \rangle$. With decreasing temperature of crystallization, homogeneous nucleation becomes stronger and finally the number of such nuclei exceeds the number of other nuclei (in plain iPP, without nucleating agents, this occurs near $T_c = 80°C$). However, the number of homogeneous nuclei formed during crystallization does not depend simply on the rate of nucleation I but on the quotient of the nucleation rate to the spherulite growth rate, I/G. In this way the quantity I/G controls $\langle R_5 \rangle$ in samples crystallized at lower crystallization temperatures.

It was found that the homogeneous nucleation rate constant I_0 for iPP is close to 9.5×10^{35} nuclei/cm^3 s, which agrees very well with the theoretical prediction[10]. In the case of homogeneous nucleation in blends calculated per unit volume of iPP in the blend, the same value of I_0 can be used.

The decrease of the homogeneous nucleation rate I in blends compared with plain iPP is caused by the decrease of the concentration of crystallizing macromolecules and by the presence of an additional energy barrier for the formation of stable nuclei in the blend. The energy barrier

is connected with the necessity of phase separation of the homogeneous blend during formation of the nuclei. The influence of this barrier on the nucleation rate in blends is much stronger than the influence of changes in concentration of crystallizing component.

The presence of aPP in the iPP/aPP blends also induces some decrease in the number of heterogeneous and self-seeding nuclei.

REFERENCES

1 Martuscelli, E. *Polym. Eng. Sci.* 1984, **24**, 1155
2 Bartczak, Z., Galeski, A., Martuscelli, E. and Janik, H. *Polymer* 1985, **26**, 1846
3 Bartczak, Z., Galeski, A. and Pracella, M. *Polymer* 1986, **27**, 537
4 Cormia, R. L., Price, F. P. and Turnbull, D. *J. Chem. Phys.* 1962, **37**, 1333
5 Gornick, F., Ross, G. S. and Frolen, L. J. *J. Polym. Sci. (C)* 1967, **18**, 79
6 Burns, J. R. and Turnbull, D. *J. Appl. Phys.* 1966, **37**, 4021
7 Koutsky, J. A., Walton, A. G. and Baer, E. *J. Appl. Phys.* 1967, **38**, 1832
8 Burns, J. R. and Turnbull, D. *J. Polym. Sci. (A-2)* 1968, **6**, 775
9 Barham, P. J., Jarvis, D. A. and Keller, A. *J. Polym. Sci., Polym. Phys. Edn.* 1982, **20**, 1733
10 Hoffman, J. D., Davis, G. T. and Lauritzen, J. I. Jr, 'Treatise on Solid State Chemistry', (Ed. N. B. Hannay), Plenum, New York, 1976, Vol. 3, Ch. 7
11 Wunderlich, B. 'Macromolecular Physics—Crystal Nucleation, Growth, Annealing', Academic Press, New York, 1976, Vol. 2
12 Clark, E. J. and Hoffman, J. D. *Macromolecules* 1984, **17**, 878
13 Blundell, D. J. and Keller, A. *J. Polym. Sci. (B)* 1968, **6**, 433
14 Stein, R. S. and Rhodes, M. B. *J. Appl. Phys.* 1960, **31**, 1873
15 Clough, S., van Aarsten, J. J. and Stein, R. S. *J. Appl. Phys.* 1965, **36**, 3072
16 Champion, G. V., Killey, A. and Meeten, G. H. *J. Polym. Sci., Polym. Phys. Edn.* 1985, **23**, 1467
17 Stein, R. S., Misra, A., Yuasa, T. and Khambatta, F. *Pure Appl. Chem.* 1977, **49**, 915
18 Yoon, D. Y. and Stein, R. S. *J. Polym. Sci., Polym. Phys. Edn.* 1974, **12**, 763
19 Prud'homme, R. E. and Stein, R. S. *J. Polym. Sci., Polym. Phys. Edn.* 1973, **11**, 1357
20 Ishikawa, T. and Stein, R. S. *Polym. J.* 1976, **8**, 369
21 Wissler, G. E. and Crist, B. *J. Polym. Sci., Polym. Phys. Edn.* 1985, **23**, 2395
22 Tabar, R. J., Wasiak, A., Hong, S. D., Yuasa, T. and Stein, R. S. *J. Polym. Sci., Polym. Phys. Edn.* 1981, **19**, 49
23 Tabar, R. J., Stein, R. S. and Rose, D. E. *J. Polym. Sci., Polym. Phys. Edn.* 1985, **23**, 2059
24 Piorkowska, E. and Galeski, A. *J. Polym. Sci., Polym. Phys. Edn.* 1985, **23**, 1723
25 Haudin, J. M. in 'Optical Properties of Polymers', (Ed. G. H. Meeten), Elsevier, London and New York, 1986, Ch. 4
26 Barham, P. J. *J. Mater. Sci.* 1984, **19**, 3826
27 Norton, D. R. and Keller, A. *Polymer* 1985, **26**, 704
28 Samuels, R. J. *J. Polym. Sci. (A-2)* 1971, **9**, 2165
29 Olabisi, O., Robeson, L. M. and Shaw, M. T. 'Polymer–Polymer Miscibility', Academic Press, New York, 1979
30 Nishi, T. and Wang, T. T. *Macromolecules* 1975, **8**, 909